Supporting information

A Hybrid Membrane-Biomimetic Nanoplatform for Synergistic Photothermal/Photodynamic Therapy of Hypoxic Tumors

Wei Chen,[a,b] Jingchao Li,[c] Haiyan Li,[d] Yifang Liu[e], Xia Lu*[a]

[a] Department of Nuclear Medicine, Northern Jiangsu People's Hospital, Clinical Medical College, Yangzhou University, Yangzhou 225001, China. Email: lxgf2222@163.com

[b] Northern Jiangsu People's Hospital, Yangzhou Clinical College, Xuzhou Medical University, Yangzhou 225001, China. Email: cw18010851397@163.com

[c] State Key Laboratory of Advanced Fiber Materials, College of Biological Science and Medical Engineering, Donghua University, Shanghai 201620, China. Email: jcli@dhu.edu.cn

[d] Department of Nuclear Medicine, Northern Jiangsu People's Hospital, Yangzhou 225001, China. Email: 18951352522@163.com

[e] Department of Clinical Pharmacology, School of Pharmacy, China Medical University, Shenyang 110122, China. Email: m13849922723@163.com

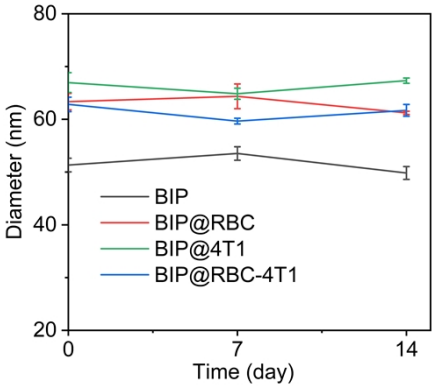

Figure S1. Changes in the hydrodynamic particle size of BIP, BIP@RBC, and BIP@4T1 BIP@RBC-4T1 monitored over 14 days (n = 3).

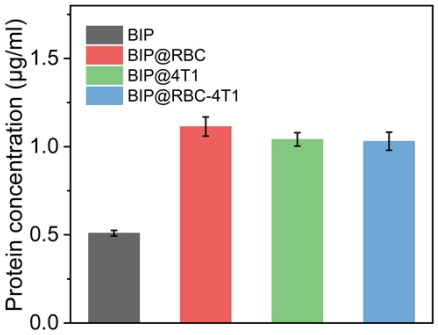

Figure S2. Detection of protein contents in SPFeN, SPFeNC, SPFeNO, and SPFeNOC using BCA kit. (n = 3).

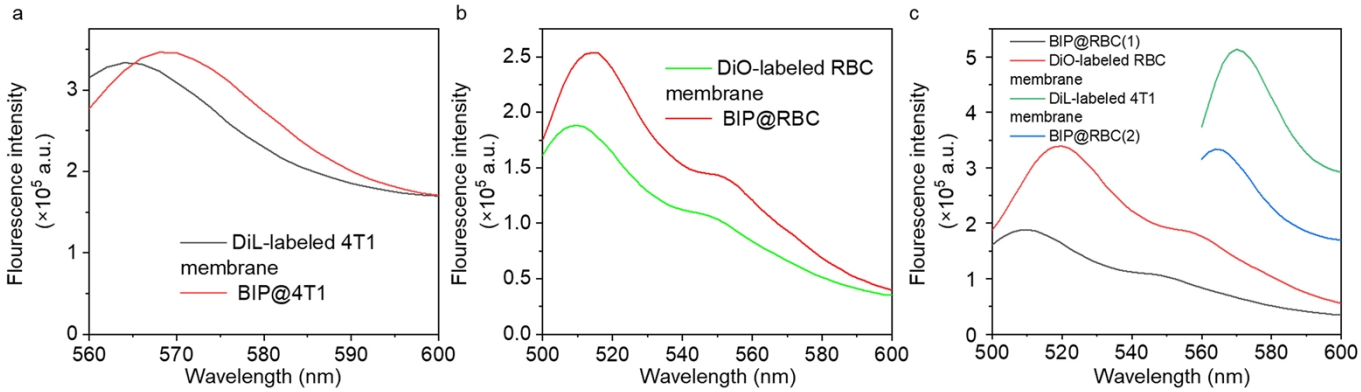

Figure S3. (a) Fluorescence spectra of DiI-labeled 4T1 cancer cell membranes and BIP@4T1. (b) Fluorescence spectra of DiO-labeled osteoclast membranes and BIP@RBC. (c) Fluorescence spectra of DiI-labeled 4T1 cancer cell membranes, DiO-labeled red blood cell membranes, BIP@RBC-4T1(1) excited by 484 nm light, and BIP@RBC-4T1(2) excited by 549 nm light.

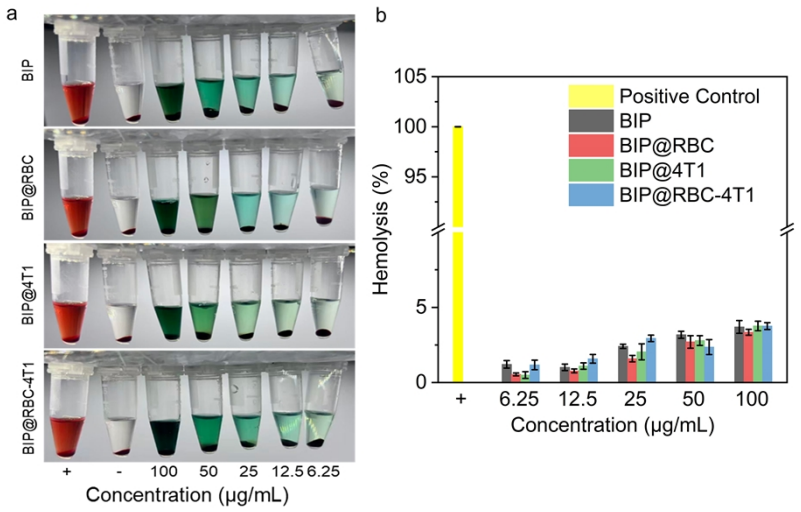

Figure S4. (a) Photographs of red blood cells after co-incubation with water (+), PBS (-), and different concentrations of BIP, BIP@RBC, BIP@4T1, and BIP@RBC-4T1. (b) Hemolysis rates of red blood cells after co-incubation with water (+), BIP, BIP@RBC, BIP@4T1, and BIP@RBC-4T1 (n = 3).

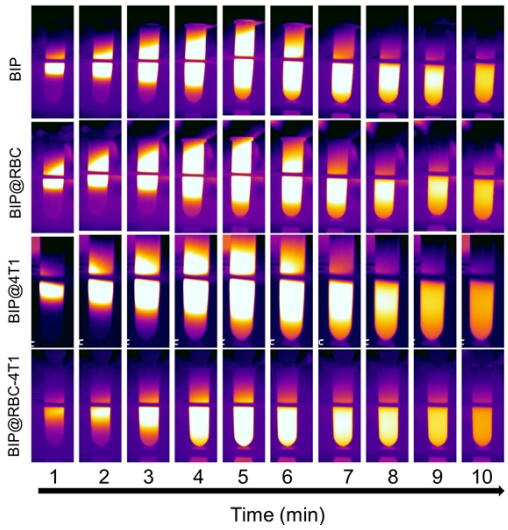

Figure S5. Thermal imaging diagrams of temperature rise of materials in each group within 10 minutes.

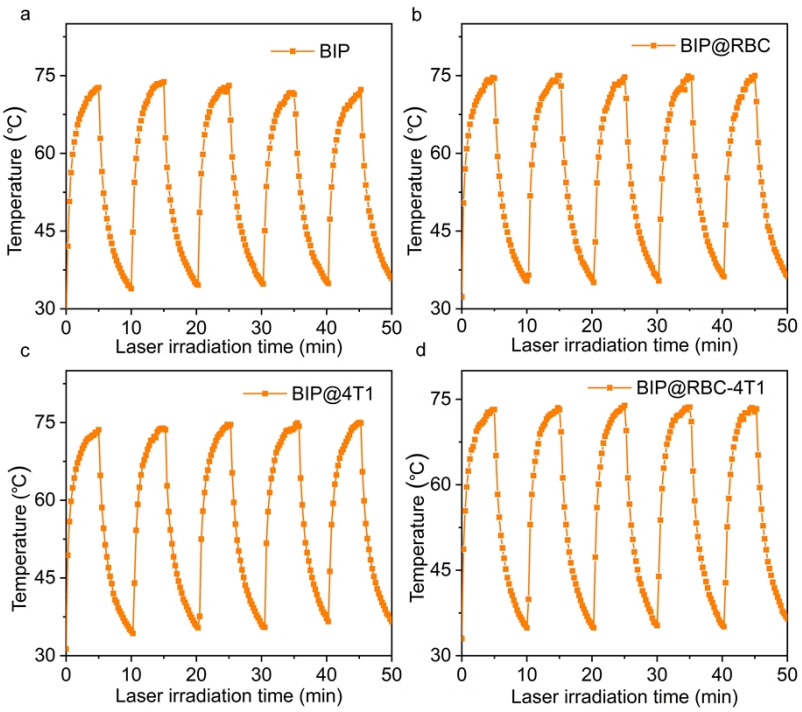

Figure S6. Temperature rise cycles of materials in each group for 5 times within 50 minutes (a) BIP group (b) BIP@RBC group (c) BIP@4T1 group (d) BIP@RBC-4T1 group.

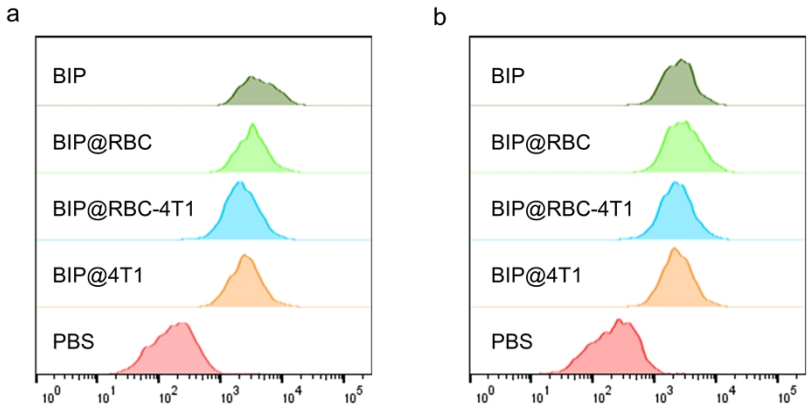

Figure S7. (a) Flow cytometry analysis of cellular uptake of BIP, BIP@RBC, BIP@4T1 and BIP@RBC-4T1 in HepG2 cells (n = 5). (b) Flow cytometry analysis of cellular uptake of BIP, BIP@RBC, BIP@4T1 and BIP@RBC-4T1 in HMEC cells (n = 5).

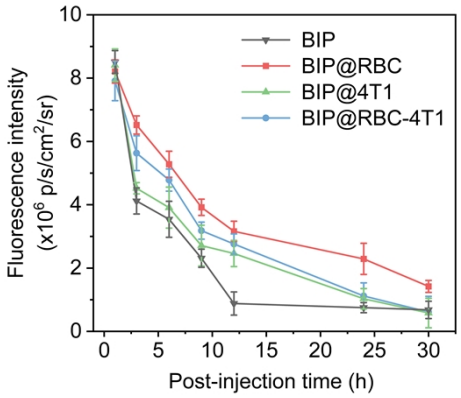

Figure S8. Fluorescence quantification in orbital venous blood of mice in each group at different time points.

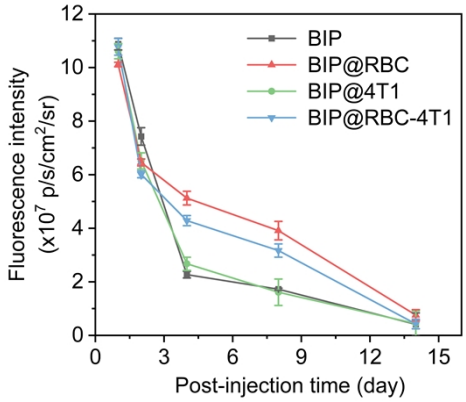

Figure S9. Fluorescence quantification in the feces of mice in each group at different time points.

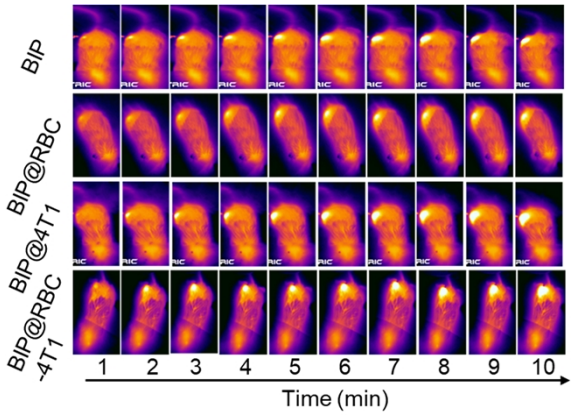

Figure S10. Thermal imaging maps of temperature rise in different groups of mice under 808 nm laser irradiation.

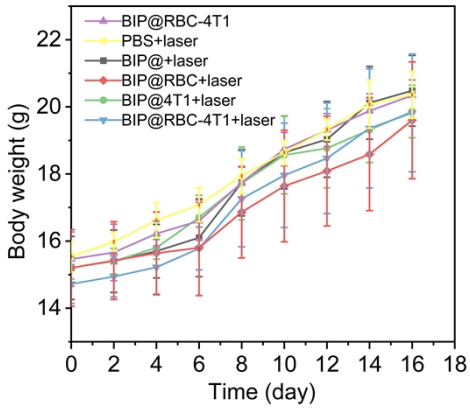

Figure S11. Body weight change curves of different groups of mice.

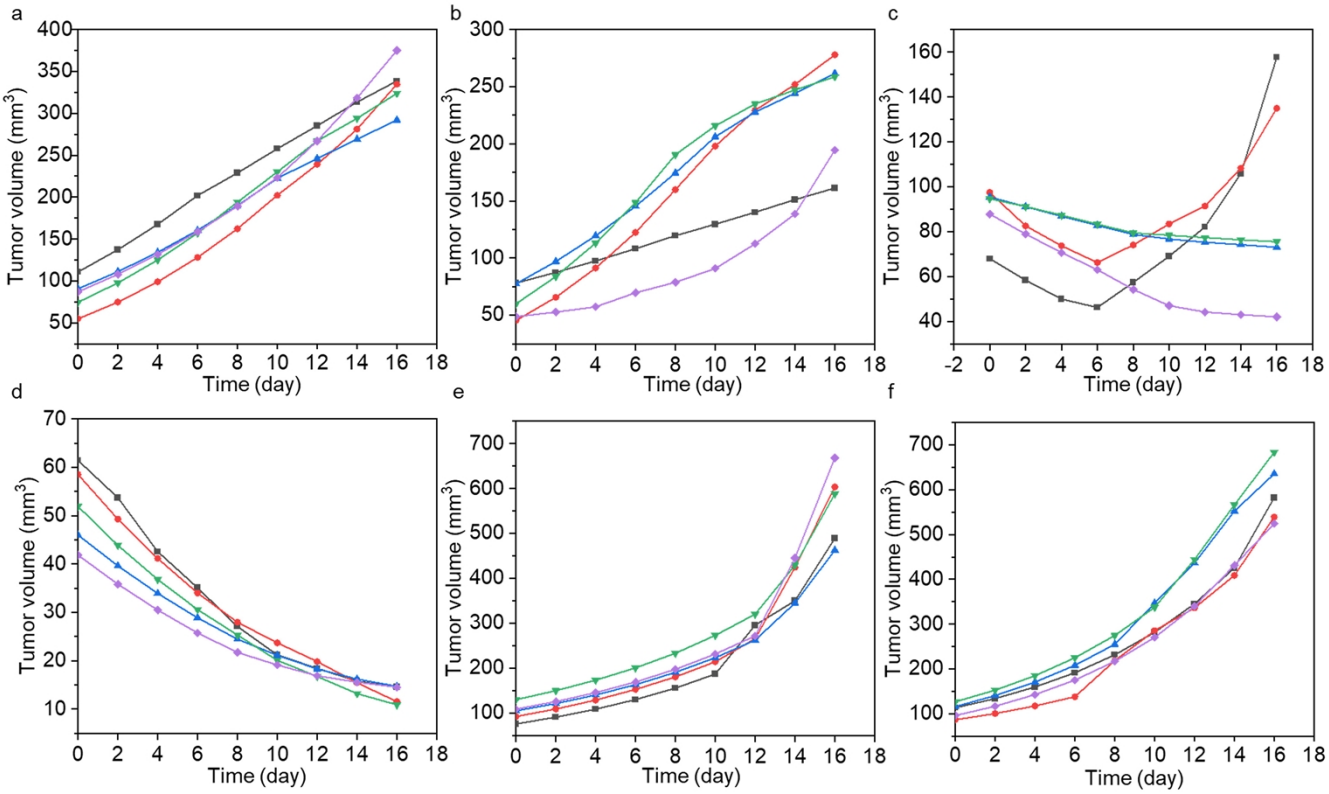

Figure S12. Tumor volumes of mice in each group after treatment (a) BIP + laser group (b) BIP@RBC + laser group (c) BIP@4T1 + laser group (d) BIP@RBC-4T1 + laser group (e) PBS + laser group (f) BIP@RBC-4T1 group.

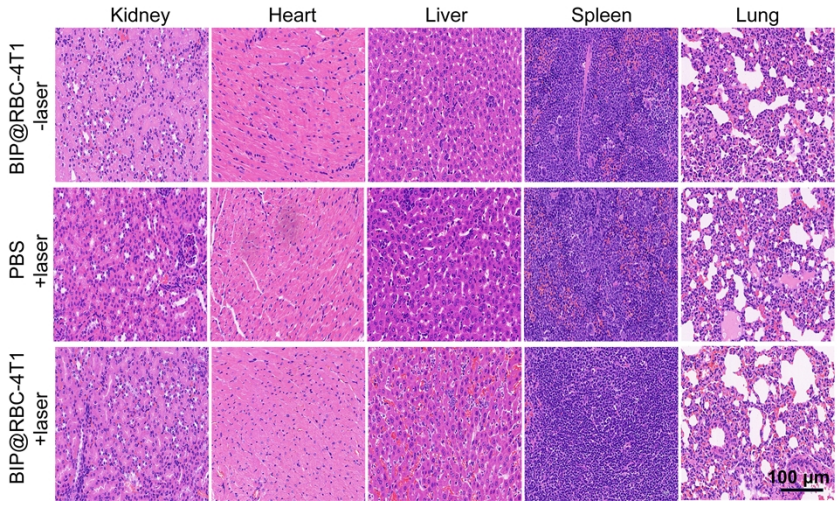

Figure S13. HE sections of heart, liver, spleen, lung and kidney organs of tumor-bearing mice in BIP@RBC-4T1-laser, PBS + laser, and BIP@RBC-4T1 + laser groups.

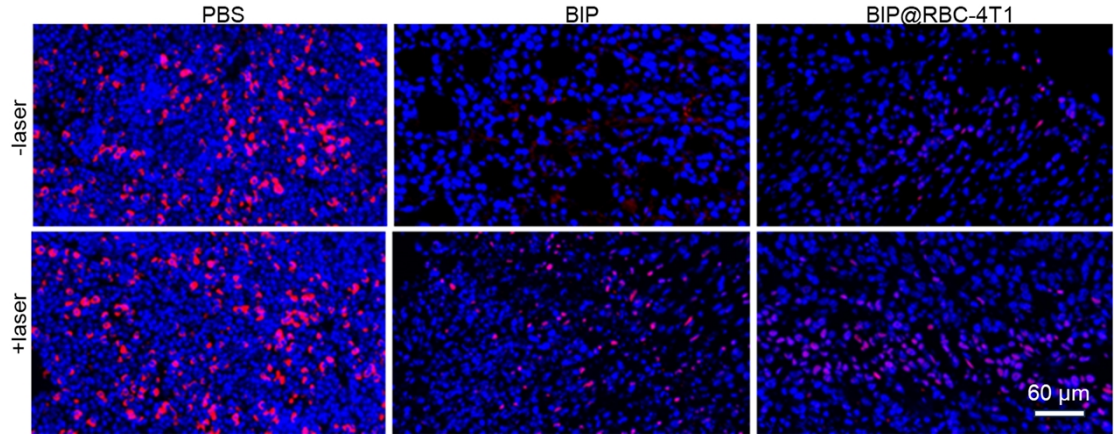

Figure S14. Immunofluorescence staining of HIF-1α in tumor-bearing mice in the PBS, BIP and BIP@RBC-4T1 group with or without treatment.